Protein Polymer MRI Contrast Agents: Longitudinal Analysis of Biomaterials In Vivo

Lindsay S. Karfeld-Sulzer,[1] Emily A. Waters,[2–5] Ellen K. Kohlmeir,[2–5] Hermann Kissler,[6] Xiaomin Zhang,[6] Dixon B. Kaufman,[6] Annelise E. Barron,[1†] and Thomas J. Meade[2–5*]

Despite recent advances in tissue engineering to regenerate biological function by combining cells with material supports, development is hindered by inadequate techniques for characterizing biomaterials in vivo. Magnetic resonance imaging is a tomographic technique with high temporal and spatial resolution and represents an excellent imaging modality for longitudinal noninvasive assessment of biomaterials in vivo. To distinguish biomaterials from surrounding tissues for magnetic resonance imaging, protein polymer contrast agents were developed and incorporated into hydrogels. In vitro and in vivo images of protein polymer hydrogels, with and without covalently incorporated protein polymer contrast agents, were acquired by magnetic resonance imaging. T_1 values of the labeled gels were consistently lower when protein polymer contrast agents were included. As a result, the protein polymer contrast agent hydrogels facilitated fate tracking, quantification of degradation, and detection of immune response in vivo. For the duration of the in vivo study, the protein polymer contrast agent-containing hydrogels could be distinguished from adjacent tissues and from the foreign body response surrounding the gels. The hydrogels containing protein polymer contrast agent have a contrast-to-noise ratio 2-fold greater than hydrogels without protein polymer contrast agent. In the absence of the protein polymer contrast agent, hydrogels cannot be distinguished by the end of the gel lifetime. Magn Reson Med 65:220–228, 2011. © 2010 Wiley-Liss, Inc.

Key words: MRI; Gd(III) contrast agent; protein polymer; hydrogel

A primary goal of tissue engineering is to regenerate biological function by combining cells and a biocompatible material with appropriate physical and biochemical stimuli to guide growth. Despite recent advances, development is hindered by inadequate techniques for material characterization (1). In in vivo studies where a biomaterial is implanted into an animal for a prescribed time, animals are sacrificed and tissues are excised for histological examination. Drawbacks of this approach include the use of numerous animals, a lack of three-dimensional data, artifacts from the animal not being alive, and the inability to perform longitudinal studies over time (2). Noninvasive imaging techniques are needed for a thorough evaluation of the properties and performance of biomaterials in vivo.

Magnetic resonance imaging (MRI) is a tomographic technique with high temporal and spatial resolution and a favorable safety profile. It is an excellent imaging modality for longitudinal noninvasive assessment of biomaterials in vivo. As MRI is sensitive to the chemical and physical environment of water molecules, it can provide information about both engineered hydrogels and the surrounding tissue. Previously, MRI has been used to image multiple properties of hydrogels in tissue engineering that include promotion of angiogenesis (3), porosity and mass transport (4,5), surrounding tissue characteristics (6–8), immune response (9–11), degradation (12–14), and drug release (15,16).

Typically, there is insufficient contrast-to-noise ratio (CNR) between an area of interest and its surroundings in an MR image. Contrast agents (CAs) address this shortcoming by increasing the relaxation rate of neighboring water protons (17). Clinically used CAs, such as gadolinium-diethylenetriaminepentaacetic acid [Gd(III)-DTPA] and gadolinium-1,4,7,10-tetraazacyclododecane-1,4,7,10-tetraacetic acid [Gd(III)-DOTA], have limited sensitivity (18). Attachment of multiple Gd(III) ions to a macromolecule amplifies the signal by increasing Gd(III) concentration and slowing molecular tumbling (19–22).

We have reported a family of multivalent, macromolecular protein polymer contrast agents (PPCAs) that have high relaxivity and are biodegradable and nontoxic (23). These PPCAs can be covalently crosslinked into the protein polymer hydrogel we have designed for tissue engineering applications (24). Because the PPCAs have high relaxivity and degrade at the same rate as the unmodified hydrogel, we hypothesized that we could noninvasively monitor the degradation of the hydrogels by MR imaging.

Here, we describe our results of imaging protein polymer hydrogels with covalently incorporated PPCAs that were implanted into mice. The substantially higher CNR of the hydrogel containing PPCA facilitates fate tracking, quantifying degradation, and the ability to distinguish the

[1]Department of Chemical and Biological Engineering, Northwestern University, Evanston, Illinois.

[2]Department of Chemistry, Northwestern University, Evanston, Illinois.

[3]Department of Biochemistry and Molecular and Cell Biology, Northwestern University, Evanston, Illinois.

[4]Department of Neurobiology and Physiology, Northwestern University, Evanston, Illinois.

[5]Department of Radiology, Northwestern University, Evanston, Illinois.

[6]Department of Surgery, Northwestern University Feinberg School of Medicine, Chicago, Illinois.

Grant sponsor: NIH/NIBIB; Grant numbers: R01EB003806 and R01EB005866; Grant sponsor: Northwestern University's NIH Biotechnology Training Grant; Grant number: 2-T32-GM008449; Grant sponsor: NIH/CCNE; Grant number: 5 U54 CA119341-02.

†*Present address:* Department of Bioengineering, Stanford University, 318 Campus Drive, W300B James H. Clark Center, Stanford, CA 94305-5444.

*Correspondence to: Thomas J. Meade, Ph.D., Northwestern University, 2145 Sheridan Road, Evanston, IL 60208-3113. E-mail: tmeade@northwestern.edu

Received 8 April 2010; revised 6 July 2010; accepted 8 July 2010.

DOI 10.1002/mrm.22587

Published online 25 August 2010 in Wiley Online Library (wileyonlinelibrary.com).

hydrogel from host tissues and in vivo immune response. These studies demonstrate that the inclusion of PPCA within the hydrogels is necessary. Hydrogels without PPCA could not be visualized toward the end of the gel lifetime, prohibiting longitudinal, noninvasive evaluation.

EXPERIMENTAL METHODS

Contrast Agent Synthesis

Protein polymer CAs were synthesized as described previously (23). The backbone of the CA was the protein polymer designated K8-120, with a sequence of GH_{10}SSG HIDDDDKHM$(GKAGTGSA)_{120}$G. The K8-120 PPCA has 120 repeats of an amino acid sequence containing lysines spaced eight amino acids apart. It was synthesized using genetic engineering and recombinant protein expression and purification with standard techniques (25). The conjugation reaction between the protein polymer and the Gd(III)-1,4,7-tris(carboxymethyl)-10-carboxybutyl-1,4,7,10-tetraazacyclododecane [Gd(III)-DO3A] chelators was performed in an aqueous buffer with 1-ethyl-3-carbodiimide hydrochloride (EDC, Fisher Scientific) and *N*-hydroxysulfosuccinimide (sulfo-NHS, Fisher Scientific). The reaction was dialyzed and lyophilized to obtain the PPCA conjugate.

Relaxivity

T_1 measurements were performed in triplicate using a Bruker mq60 NMR Analyzer (Bruker Canada, Milton, ON, Canada) at 60 MHz (1.5 T) and 37°C at three concentrations. Inductively coupled plasma atomic emission spectrometry (ICP-AES) on a Varian VISTA-MPX ICP spectrometer (Palo Alto, CA) at Northwestern University's IMSERC was used to measure Gd(III) concentration. Relaxivity was determined by fitting the slope of $1/T_1$ versus Gd(III) concentration.

Hydrogel Formation

Hydrogels were prepared by enzymatic crosslinking of two protein polymers, K8-30 [GH_{10}SSGHIDDDDKHM$(GK AGTGSA)_{30}$G] and Q-6 (GH_{10}SSGHIDDDDKHM [$(GQQQL GGAGTGSA)_2(GAGQGEA)_3]_6$G) with and without the K8-120 PPCA. The K8-30 and Q-6 proteins were cloned, expressed, and purified using the same methods as described for the K8-120 protein polymer (25) but were further purified by phase separation to remove endotoxins. It was not necessary to remove endotoxins for the K8-120 PPCA because the small concentrations used in the experiments constituted a negligible amount.

Endotoxins were removed through multiple rounds of a phase separation method optimized from a literature protocol (26). Triton X-114 (Sigma) was added at 1% to protein dissolved at 10 mg/mL in endotoxin-free water, and the pH was adjusted to ~9.5. The solution was stirred for 30 min at 4°C, placed in a 37°C water bath for 10 min, and centrifuged at 10,000*g* at 37°C for 10 min. The supernatant containing the protein was placed into a new conical tube, and the process was repeated multiple times, with pH readjustment to ~9.5 after every four rounds. Following the last round of phase separation, the solution was placed on degassed Bio-beads SM2 Adsorbents (Bio-rad Laboratories, Hercules, CA) to remove any remaining Triton X-114. Samples were dialyzed against endotoxin-free water and lyophilized. The endotoxin levels were tested using a QCL-1000 Endpoint Chromogenic LAL assay (Lonza, Walkersville, MD). Proteins were only used if the endotoxins (EU) per mL of protein when dissolved at concentrations used in the hydrogels were less than 20 EU/mL.

Tissue transglutaminase (tTG) from guinea pig liver (Sigma) was used to crosslink the protein polymers into hydrogels. tTG was dissolved at 0.04 U/μL in 2 mM ethylenediaminetetraacetic acid (EDTA), 20 mM dithiothreitol, pH 7.7. The lysine-containing protein, K8-30, was dissolved at 10 wt % in 200 mM 4-morpholinepropanesulfonic acid (MOPS), 20 mM $CaCl_2$, pH 7.6. The glutamine-containing protein, Q-6, was resuspended at 15 wt % in 2 mM EDTA, pH 7.3. The three components were combined at a ratio of 1:1.5:1.5 for tTG:K8-30:Q-6 solutions. K8-120 CA was dissolved at 10 wt % in 200 mM MOPS, 20 mM $CaCl_2$, pH 7.6. When K8-120 CA was included, the K8-30 volume was decreased by a corresponding amount to maintain constant hydrogel volume. Protein polymer precursors with enzyme were mixed with brief vortexing and incubated at 37°C until gelation occurred (minutes).

Fluorophore-labeled K8-30 was included at 1% of the total hydrogel volume to validate the presence of the hydrogel with histology. To synthesize this conjugate, the Alexa-Fluor 488 5-TFP dye (excitation wavelength = 496 nm, emission wavelength = 519 nm, Invitrogen) was coupled with the K8-30 protein polymer. The protein polymer was dissolved at 1.16 mg/mL in 0.1 M sodium bicarbonate, pH 9.0, and the AlexaFluor 488 5-TFP was dissolved at 1 mg/μL in DMF. A total of 50 μL of the AlexaFluor solution was added to 5 mL of protein polymer solution. The reaction was incubated at room temperature with continuous stirring for 1 h. Unreacted fluorophore and salt were removed using a CENTRI-SEP spin column (Princeton Separations, Adelphia, NJ). The average number of conjugated fluorophores was estimated by MALDI-TOF spectrometry. This conjugate was dissolved at 10 wt % in 200 mM MOPS, 20 mM $CaCl_2$, pH 7.6, for inclusion in the hydrogel.

The Gd(III) concentration in the hydrogel samples was analyzed by inductively coupled plasma mass spectrometry (ICP-MS) on a Thermo Electron Corporation (Waltham, MA) XSeriesII ICP-MS with Thermo PlasmaLab software. All Gd(III) standards and samples contained 5 ng/mL of a multielement internal standard (Spex CertiPrep, Metuchen, NJ) consisting of Bi, Ho, In, Li, Sc, Tb, Y, and 3% nitric acid (v/v).

In Vitro Hydrogel Imaging

Gels with 0.1 mM Gd(III) of K8-120 PPCA were imaged on a 4.7 T Bruker Biospec 4740 MR system using a 38 mm diameter birdcage coil (Rapid MRI, Columbus, OH) without temperature control. A spin echo pulse sequence was used with TR = 100 msec, TE = 14.5 msec, 20 signal averages, and a 0.12 × 0.12 × 1 mm^3 resolution. To calculate

T_1, an accelerated variable TR pulse sequence (RARE-VTR) was used with TE = 9.8 msec, TR = 131.5, 250, 400, 550, 750, 1050, 1550, and 3750 msec, two signal averages, and a 0.12 × 0.12 × 1 mm^3 resolution. T_2 values were measured using a multiecho sequence with TR = 2000 msec, TE = 15–240 msec (intervals of 15 msec), one signal average, and a 0.12 × 0.12 × 1 mm^3 resolution.

In Vivo Studies

All animal procedures were approved by Northwestern University's and Northshore University HealthSystem's Institutional Animal Care and Use Committees. Hydrogels with a total volume of 50 μL were preformed and surgically implanted subcutaneously on the hind flanks of age-matched C57/BL6 mice. Mice were continuously anesthetized with 2% isoflurane, and the surgical area was shaved and wiped with alcohol. Incisions were parallel to the spine, and a pocket was created by blunt dissection to allow insertion of the hydrogel. Monocryl 5-0 sutures (Esutures, Mokena, IL) were used to close incisions.

In Vivo MR Imaging

For each imaging experiment, mice were anesthetized using 2% isoflurane, and respiration was monitored using a pressure sensor. Anesthesia was adjusted as needed to maintain a respiratory rate of 60–90 breaths/min. The mice were serially imaged over a period of up to 22 days after surgery using the same imaging protocol employed for the in vitro image acquisition (4.7 T magnet with birdcage coil without temperature control). After preliminary coronal and axial images were acquired to localize the graft, a series of fat-suppressed images were measured.

To compare relaxation times in the hydrogels (pre- and postimplantation), mice were implanted with the same hydrogels that were imaged in vitro. Mice were imaged immediately after surgery and again 1 day later. To measure T_1s, a RARE-VTR pulse sequence with eight TRs from 115 to 3750 msec was used with TE = 12.5 msec, one signal average, and a 0.16 × 0.16 × 1 mm^3 resolution. T_2 values were measured using a multiecho sequence with TR = 2000 msec and 16 echoes with TE = 20–400 msec, one signal average, and a 0.16 × 0.16 × 1 mm^3 resolution.

In Vivo Detailed Degradation Curve

For a detailed assessment of hydrogel degradation, 0.3 mM Gd(III) PPCA-containing hydrogels were implanted into three mice, and they were imaged every 3–5 days for up to 20 days after implantation. A MSME spin echo pulse sequence was used with TR/TE = 500/14.5 msec, 4 cm FOV, 256 × 256 matrix, 1 mm slice thickness, and two signal averages. Both coronal and axial stacks were acquired to fully cover the grafts.

In Vivo Time Course

Eight mice were implanted with two hydrogels each: a hydrogel without PPCA on the mouse's left side and with 0.2 mM Gd(III) PPCA on the right. All imaging was performed with a 4 cm FOV and 256 × 256 matrix, and gain settings were constant for each type of scan for each mouse over the entire time. Imaging was conducted to evaluate hydrogel degradation, CNR, and T_1 values over time. Stacks of axial slices with a MSME spin echo pulse sequence with 8–10 0.5 mm thick slices and TR/TE = 285/14.6 msec were acquired to analyze graft volumes. Gradient echo images were acquired to analyze CNR and were run with the following parameters: TR/TE = 100/4.1 msec, two axial 1 mm slices (one slice through the center of each hydrogel), 4 cm FOV, 256 × 256 matrix, and 20 signal averages. T_1 values were measured using a RARE-VTR sequence with TE = 9.8 msec, TR = 255, 370, 505, 670, 881, 1177, 1673, and 3750 msec, two 1 mm slices (the same slices used for CNR measurements), 4 cm FOV, 256 × 256 matrix, and two signal averages.

Image Analysis

Images were analyzed using ImageJ software (National Institutes of Health, Bethesda, MD). Additionally, 3D reconstructions of the grafts were constructed in Amira 4.0 software (Visage Imaging, Inc., Andover, MD). To calculate the volume, the graft was manually planimetered on each slice, and the areas were summed and multiplied by the slice thickness. Only bright central areas were included in volume calculations, omitting any surrounding ring of lighter intensity (which was interpreted as inflammatory response).

Data from multiple TR and multiple TE scans (to calculate T_1 and T_2 values, respectively) were fit with Origin 7 (OriginLab Corporation, Northampton, MA) using the following equations:

$$S_i = S_0\left(1 - \exp\left(-\mathrm{TR}\Big/T_1\right)\right) \quad [1]$$

$$S_i = S_0 \exp\left(-\mathrm{TE}\Big/T_2\right), \quad [2]$$

where S_0 is a constant and S_i is the signal intensity at a particular TR or TE.

Gradient echo images were analyzed for the signal intensity of the hydrogel with PPCA, the hydrogel without PPCA, and skeletal muscle as an internal control (constant across mice and time). Additionally, the standard deviation (SD) of the signal intensity of the background was measured. CNR was calculated relative to skeletal muscle using the following equation:

$$\mathrm{CNR} = \frac{\mathrm{SI_H} - \mathrm{SI_M}}{\mathrm{SD}}, \quad [3]$$

where SI_H is the signal intensity of the hydrogel and SI_M is the signal intensity of skeletal muscle.

Histology

At each time point, one or two mice were sacrificed for histological examination. Implants were excised and placed immediately in 10% neutral buffered formalin (Fisher Scientific). Samples were processed on a Leica TP 1050 tissue processor (Leica Microsystems, Germany) and paraffin embedded on a Sakura Tissue Tek

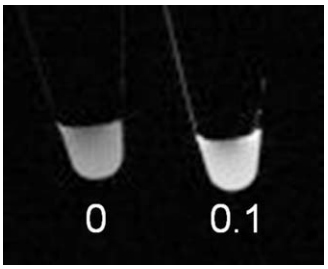

FIG. 1. MR images at 4.7 T of hydrogels containing 0 mM Gd(III) and 0.1 mM Gd(III) of the K8-120 PPCA. Imaging parameters: TR/TE = 100/14.6 msec, 128 × 128 matrix, 3 cm FOV, 1 mm slice thickness, and 20 signal averages.

embedding unit (Sakura Finetek U.S.A., Torrance, CA). Sections were cut at 5 μm thickness on a Leica 2135 microtome (Leica Microsytems). Slides were stained with hematoxylin and eosin (H&E) with standard procedures, and all materials were purchased from Sigma. Masson's trichrome staining (Sigma) was performed according to standard protocols to detect collagen capsule formation. Sections were examined by immunohistochemistry to distinguish macrophages using a Mac-3 antibody, clone M3/84 (BD Pharmingen, San Jose, CA), dilution 1:200, with a biotinylated secondary antibody/streptavidin horseradish peroxidase/3,3′-diaminobenzidine system (Dako, Carpinteria, CA). Slides were imaged using a Nikon Eclipse 50i upright microscope (Nikon, Melville, NY), and pictures were taken with Spot Advanced software (Diagnostic Instruments, Sterling Heights, MI) in Northwestern University's Institute for Bionanotechnology and Medicine. A mercury lamp with a 492–518 nm excitation wavelength and a 532–536 emission filter was used to image fluorescently labeled gels on unstained slides.

Statistical Analysis

Statistics were performed using Origin 7 (OriginLab Corporation, Northampton, MA) with a one-tailed, two-sample *T* test. A *P* value less than 0.05 was considered significant.

RESULTS

In Vitro Hydrogel Imaging

The synthesized K8-120 PPCA contained ~39 Gd(III)-DO3A chelators, representing a conjugation efficiency of 32%. The relaxivity was 15.1 mM^{-1} sec^{-1} per Gd(III) and 584.4 mM^{-1} sec^{-1} per molecule at 37°C and 1.5 T. Protein polymer hydrogels, with and without 0.1 mM Gd(III) of the K8-120 PPCA, were imaged on a 4.7 T magnet. The hydrogels containing the PPCA have greater signal intensity on a T_1-weighted image (Fig. 1). Signal intensity differences correlate with T_1 relaxation times at 4.7 T, with the PPCA-containing hydrogel having a T_1 relaxation time of 354 ± 2 msec, significantly shorter than the non-PPCA-containing hydrogel's T_1 of 716 ± 4 msec ($P < 0.01$) (Table 1). The T_2 relaxation times are also significantly different ($P < 0.01$), with the PPCA-containing hydrogel's value 2.7 times lower.

T_1 and T_2 Values of Hydrogels Before and After Implantation

The hydrogels imaged in vitro were subcutaneously implanted into mice and imaged immediately and again 1 day later. As shown in Table 1, the T_1 values significantly increase from before implantation to immediately after implantation and again 1 day after implantation (an overall 69% increase). On the other hand, T_2 values vary less, with only a 21% overall increase.

Detailed Degradation Curve

To obtain a detailed degradation curve, 50 μL PPCA-containing hydrogels were implanted subcutaneously in three mice and imaged at a high frequency, every 3–5 days. The hydrogel implanted into mouse 1 fractured before implantation, resulting in a smaller gel. The hydrogels almost completely degrade over the course of 20 days (Fig. 2). By measuring the area of the hydrogel in each slice, followed by multiplying by the slice thickness (and summing over all slices), the implant volume is obtained and degradation can be quantified (Fig. 2c). For each mouse, there is a lag time of ~6 days where no apparent degradation occurs, followed by a linear degradation rate of 4.2 ± 0.6 mm^3/day. Toward the end of the experiment, it appears that the degradation rate slows.

Time Course

A time course series study was performed to obtain statistically relevant data for degradation, CNR, and T_1 relaxation times. Imaging time points immediately after implantation and corresponding to the beginning, middle, and end of degradation were determined from the degradation curve. These points corresponded to 1, 8, 15, and 22 days after implantation. Both the implant volume and the contrast decreased over time, as shown in Fig. 3. The volume was calculated for the hydrogels containing PPCA using 0.5 mm slices (Fig. 4).

Table 1
T_1 and T_2 Relaxation Times for Hydrogels as Measured on a 4.7 T Imager

	T_1[a]		T_2[a]	
	CA	No CA	CA	No CA
Hydrogel before implantation	354 ± 2	716 ± 4	45.9 ± 1.1	124.1 ± 1.4
Immediately after implantation	452 ± 12	910 ± 13	45.6 ± 0.8[b]	157.9 ± 2.5[b]
One day after implantation	601 ± 60	1152 ± 6	52.1 ± 1.8[b]	149.3 ± 2.2[b]

[a]All times are in msec. $n = 2$ except where noted.
[b]$n = 1$.

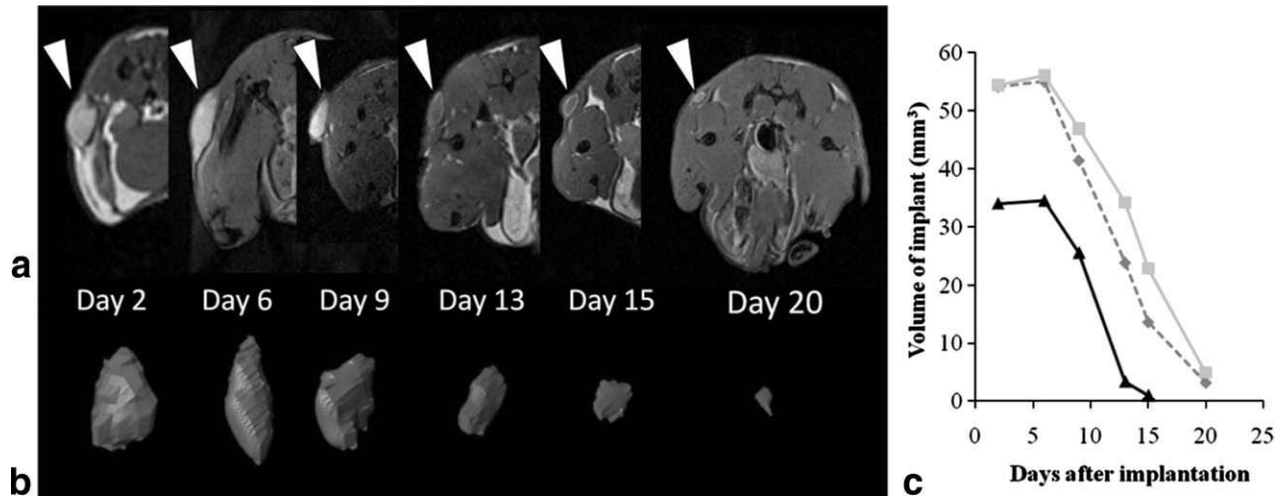

FIG. 2. Detailed degradation curve of a PPCA-containing hydrogel implanted subcutaneously in three mice. Images were acquired every 3–5 days on a 4.7 T magnet with a MSME spin echo pulse sequence. **a**: Axial spin echo images of mouse 2. **b**: 3D reconstructions of the grafts in mouse 2. **c**: Calculated volume versus time using an average of coronal and axial images for mouse 1 (▲), mouse 2 (◆), and mouse 3 (■).

CNR was compared between the hydrogels with and without PPCA. Hydrogels with PPCA have a much higher CNR for all time points ($P < 0.05$) (Fig. 5). With PPCA, hydrogels initially have a CNR of 74.8, which drops to 23.5 by day 22. Hydrogels without PPCA have an initial CNR of 33.0, less than half of the value with PPCA; it decreases to 3.4 at day 22.

T_1 relaxation times corresponded to intensities seen in the images. A ring was observed around the hydrogel in the MR images that was hypothesized to be inflammation (discussed in detail in the next section). Measurements were taken of both the hydrogel and this surrounding area. At day 1 there was no apparent inflammation surrounding the gels and thus, no measurement was taken. At each time point, the T_1 of the hydrogel with PPCA was significantly lower than without PPCA, and the T_1 of both hydrogels increased from day 1 to day 22 (Fig. 6). The inflammation surrounding the gels had a significantly longer T_1 than all the gels except the non-PPCA gel at day 22. At days 8 and 15, the T_1 of the area surrounding the PPCA-containing hydrogels is significantly shorter than the area adjacent to the non-PPCA-containing gels. Between day 1 and day 8, the T_1 of the PPCA-containing gel remains approximately the same but is significantly longer at each of the next two time points.

Imaging Immune Response

During the course of the in vivo studies, none of the animals appeared sick or died unexpectedly, indicating the implants were nontoxic. However, there was a visual indication of a local immune response from the implants, with round protrusions at the site in some animals. At each time point, at least one animal was sacrificed, and both implants were excised for histological examination and validation of the MR images. H&E-stained histology samples that show significant immune cell infiltration correspond well to acquired MR images of the implanted gels with a surrounding layer (Fig. 7a–h).

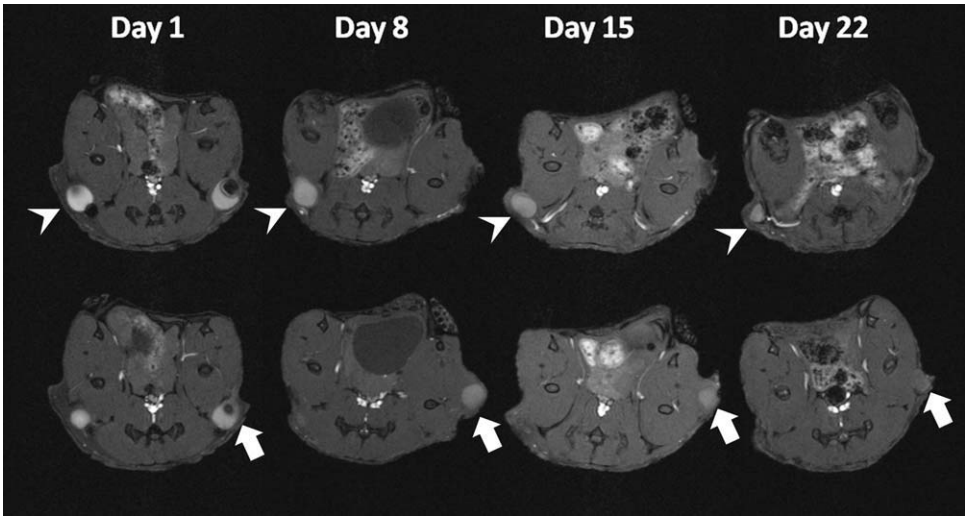

FIG. 3. Gradient echo images on a 4.7 T magnet of the same mouse at 1, 8, 15, and 22 days after hydrogels were implanted. Arrowheads indicate the hydrogel with PPCA and arrows indicate the hydrogel without PPCA. Volume and CNR of implants decrease over time; hydrogels with PPCA have greater CNRs throughout the time series. Imaging parameters: TR/TE = 100/4.1 msec, 1 mm slice thickness, 256 matrix, 4 cm FOV, and 20 averages.

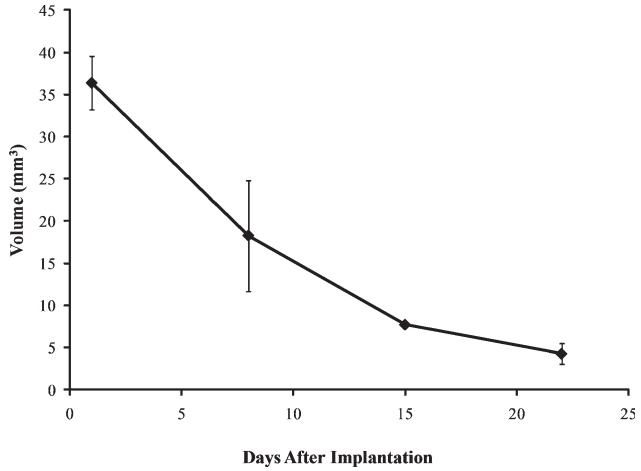

FIG. 4. Volume of hydrogel implants with 0.2 mM K8-120 PPCA as measured with MR images at 4.7 T. Each volume is statistically greater than the subsequent volume with $P < 0.01$. Images were acquired with 0.5 mm slices, TR/TE = 285/14.6 msec, 4 cm FOV, 256 matrix, and four signal averages.

The hydrogels could be positively identified in histology images by including fluorophore-conjugated K8-30 (Fig. 7i). After 1 day, immune cell infiltration was minimal, with a small layer of cells and no fibrinous exudate, and there is no ring of lighter intensity in the corresponding MR image. However, at the next time point (8 days after implantation), a dense polymorphonuclear leukocyte infiltration and a ring of fibrinous exudate appear that persisted through the last time point at 22 days after implantation. The corresponding MR images at 8, 15, and 22 days had a lighter area around the gels, whether or not they contain CA. In addition to H&E staining, both Mac-3 staining for macrophages and Masson's trichrome staining for collagen all demonstrated a significant immune response to the hydrogels. Over time, there is greater macrophage presence (indicated by a brown color) and the formation of a collagen capsule (indicated by a blue ring), as demonstrated with histological images at day 22 (Fig. 7j–l).

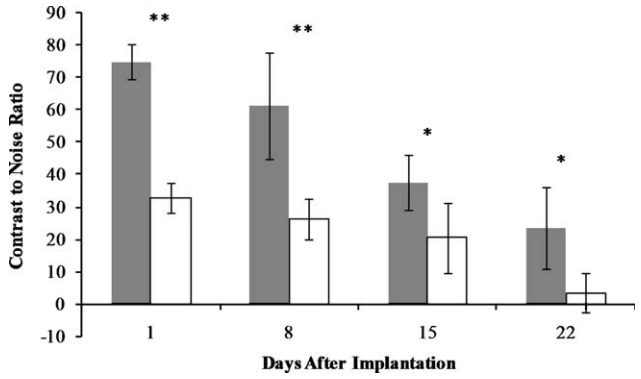

FIG. 5. Contrast-to-noise ratio of hydrogel to skeletal muscle. Gray bars: hydrogels with PPCA. White bars: hydrogel without PPCA. A statistically significant difference with $P < 0.01$ is denoted with ** and $P < 0.05$ is denoted by *.

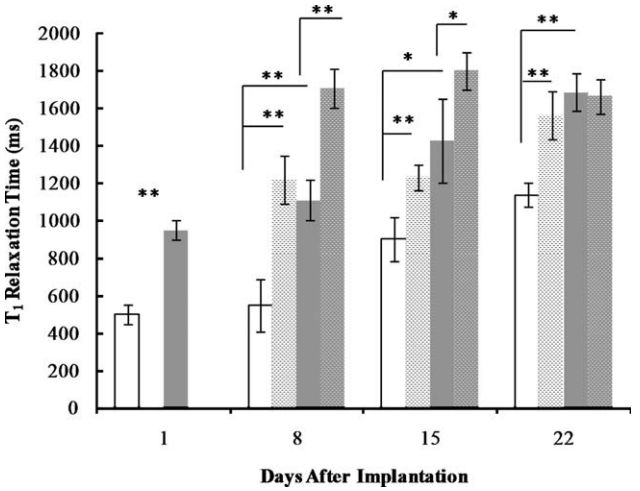

FIG. 6. Comparison of T_1 relaxation times over 22 days for hydrogel graft with PPCA (white), hydrogel graft without PPCA (gray), inflammatory area surrounding hydrogel with PPCA (white hashed), and inflammatory area surrounding hydrogel without PPCA (gray hashed). A statistically significant difference with $P < 0.01$ is denoted with ** and $P < 0.05$ is denoted by *.

DISCUSSION

MRI has the potential to noninvasively image biomaterials if sufficient contrast difference between the biomaterial and the surrounding tissues is evident. We have demonstrated that incorporating PPCAs into a hydrogel provides enhanced contrast over the in vivo lifetime of the materials. We have shown the ability to track the hydrogel, quantify degradation, and detect and observe an immune response over time. Although the hydrogel is initially visible without PPCA, it becomes indistinguishable from the surrounding tissue after some degradation. Therefore, it is necessary to include PPCA to image implanted hydrogels for in vivo fate mapping.

The K8-120 PPCA used in these experiments, a bioconjugate of a protein polymer with Gd(III) chelators covalently attached through lysine side chains, has previously been characterized (23). The protein polymer contains 120 repeats of the amino acid sequence, GKAGTGSA, providing 121 (120 lysines in the repeats and one in a 10x histidine tag) possible sites for the hepta-coordinated Gd(III)-DO3A chelator. An amide bond formation reaction between the free amines on the lysine side chain and a carboxyl group on the chelator yields the conjugate. Because the conjugation reaction is performed in an aqueous buffer, there was a low efficiency that resulted in only 39 chelators in the conjugate PPCA.

Although the uncrosslinked K8-120 PPCA had a very high relaxivity in water at 1.5 T and 37°C, it was difficult to predict a priori how much contrast would be evident in a hydrogel at room temperature and 4.7 T. As demonstrated in the in vitro hydrogel images, the K8-120 PPCA enhanced the contrast within an enzymatically crosslinked protein polymer-based hydrogel when imaged at 4.7 T and room temperature (field strength, temperature, macromolecular content, and the effects of crosslinking into a hydrogel all affect contrast in a MR image).

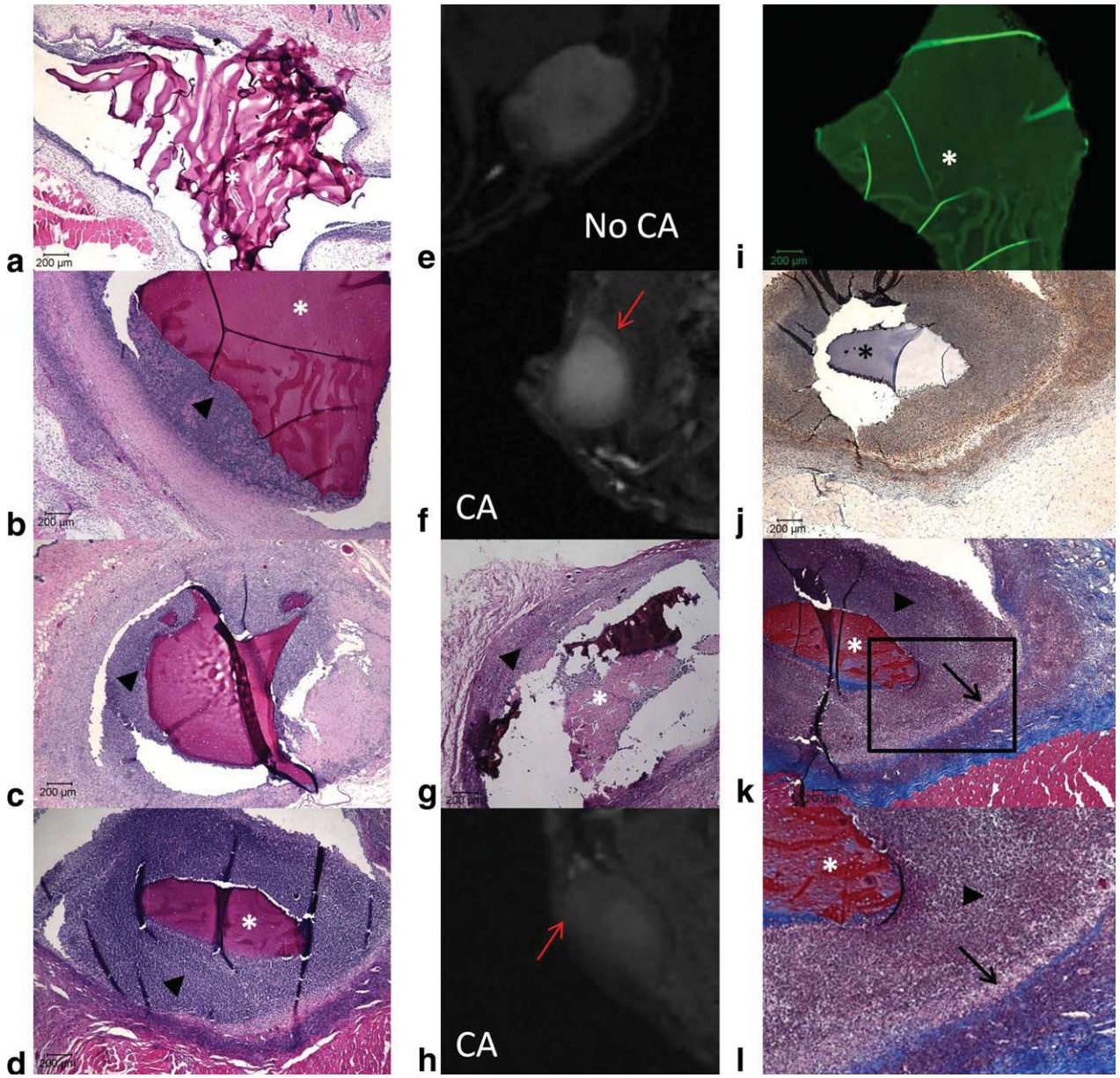

FIG. 7. Histology and MR images of excised implants. **a, e**: Day 1, no PPCA; **b, f, i**: day 8, with PPCA; **c**: day 15, no PPCA; **g**: day 15, with PPCA; **d, h, j, k, l**: day 22, with PPCA. **a–d, g**: H&E-stained images with 4× magnification; **e, f, h**: corresponding gradient echo MR images with TR/TE = 100/4.1 msec and with red arrow marking lighter area of inflammation; **i**: unstained image confirming hydrogel; **j**: Mac-3 staining at 4× magnification of PPCA implant at 22 days; **k**: Masson's trichrome staining at 4× magnification of PPCA implant at 22 days; **l**: enlarged close-up of Masson's trichrome staining. * indicates the implant, arrowheads mark polymorphonuclear leukocyte infiltration, red arrow marks lighter area of inflammation, and black arrow points to the collagen capsule.

Both the high concentration of the protein polymers and the resulting elevated viscosity affect observed contrast because macromolecular content and greater viscosity both increase relaxivity (2,27). As shown in Fig. 1 and Table 1, the hydrogel without CA has significant contrast and a relatively low T_1 and is most likely due to the high protein content and the gel properties. The relaxation properties of the PPCA in a gel can differ in solution because of multiple factors, including rate of water exchange, water access, and rotational correlation time. The contrast observed in the phantom images correlates well to the T_1 relaxation times. The PPCA-containing hydrogel's T_1 is approximately half that of the non-PPCA-containing hydrogel; however, both values are significantly lower than water ($T_1 \geq 2500$ msec).

Imaging the hydrogels before and immediately after implantation shows that the T_1 values increase between the in vitro and in vivo placement. The T_1 of both hydrogels increased ~27% on implantation and an additional 30% 1 day later. The T_1 of the hydrogel with PPCA was consistently lower, with the ratio of the unlabeled to labeled hydrogel T_1s remaining at ~2. Changes in temperature and solvent and solute flux may explain these differences in T_1 over time. Other data indicate that

degradation and inflammation are not significant after 1 day and should only minimally affect T_1 values.

The results demonstrate the ability to track hydrogels in vivo over time by incorporating PPCAs. Imaging mice every 3–5 days allowed preparation of a detailed degradation curve by calculating the graft volume at each time point. These data were used to choose appropriate imaging times for subsequent studies to capture initial, intermediate, and end points of the apparent degradation curve. The gel volumes were tracked using the hydrogels with PPCA. Although both hydrogels have enough contrast at earlier time points, the gels without PPCA are difficult to distinguish from surrounding tissue at later time points. We have assembled a degradation curve using volumes averaged across all mice with relatively low SDs. The average volume at each time point remains statistically greater than the subsequent volume ($P < 0.01$).

The degradation rate of biomaterials is a critical parameter in tissue engineering and influences the tissue morphogenesis as the physical properties of the hydrogel change as it breaks down. Both mesh size and swelling increase as degradation progresses, which concomitantly influence diffusion and mechanical strength (28). Several studies have highlighted the importance of hydrogel degradation rate on the formation and assembly of extracellular matrix (ECM) and structurally sound tissues (29–31). Ideally, the material degradation synchronizes with the tissue growth; a deposited ECM can replace the biomaterial (32). The degradation rate can also have an impact on the immune response through changes in shape, porosity, release of harmful degradation products, and surface roughness (33). For in situ gelling materials, it is also advantageous to be able to track, spatially, the initial deposition of the hydrogel (34).

The importance of including the PPCA within the hydrogel is illustrated by the difference in CNR. At each time point, the CNR for PPCA-containing hydrogels is at least 1.6 times greater than non-PPCA-containing hydrogels. By 22 days after implantation, the CNR without PPCA is so low that it is not possible to distinguish between the hydrogel and the surroundings. By incorporating the PPCA, the difference in signal strength between the hydrogel and the surrounding tissue is augmented, providing more distinct boundaries to properly identify the hydrogel.

The contrast difference is confirmed by the analysis of T_1 relaxation times of the hydrogels and the surrounding tissue. Throughout the duration of the study, the T_1 of the PPCA-containing hydrogel is significantly different from the surrounding inflamed tissue. However, without the PPCA, the T_1 of the hydrogel and the surrounding area is the same by day 22.

At days 8 and 15, the T_1 of the surrounding tissue is greater when no PPCA is present, so it is possible that some degraded PPCA has diffused out of the gel, lowering the T_1 of the area adjacent to the PPCA-containing hydrogel. The difference in T_1 over time also indicates how the degradation affects the PPCA within the center of the hydrogel, as the T_1 increases over time. As demonstrated previously, the high relaxivity of the PPCA is due to the long length of its protein backbone; thus, degradation would increase the T_1 (23).

In the assessment of all parameters, it must be noted that as it becomes difficult to distinguish the hydrogel, the measured regions of interest may not be accurately defined without PPCA. This shortcoming also highlights the necessity of the PPCAs.

MRI has previously been used to image the host response of a biomaterial, correlating relaxation times and signal intensity to an inflammatory response (2,9–11,35). However, to the best of our knowledge, this is the first time that the foreign body response of a biomaterial has been detected using a Gd(III)-based CA. By shortening the T_1 of the hydrogel, the PPCA distinguishes the implant from the surrounding inflammatory tissue. Histology shown here confirms that a ring surrounding the protein polymer hydrogels in MR images is due to an immune response that is characterized by polymorphonuclear leukocyte infiltration and a fibrinous exudate (Fig. 7).

As illustrated in the histology and corresponding MR images, there was a significant inflammatory response to the protein polymer hydrogels both with and without PPCA. Because the PPCAs were not purified for endotoxin removal, it is possible that the small amount of endotoxins contributed from the PPCAs increased the immune response in the PPCA-containing hydrogels. However, this potential effect was overwhelmed by other influences. These results indicate that these hydrogels are immunogenic in the formulation used in these experiments.

This immune response persists through the end of the study, and later time points show increased macrophage presence and the formation of a collagen capsule. These results are typical of a foreign body response to a biomaterial (36). As demonstrated here, the PPCA enables clear distinction of the hydrogel from the surrounding inflammatory tissue. The biocompatibility of a biomaterial is a critical property, and discriminating between the hydrogel and the tissue in an MR image improves the accuracy of the assessment.

CONCLUSION

The inclusion of the K8-120 PPCA in protein polymer hydrogels enables in vivo analysis of critical properties of the biomaterial over time through MRI. Fate mapping, quantification of degradation, and detection of a foreign body response are facilitated through the incorporation of PPCA. By displaying a CNR that is 2-fold greater than hydrogels that do not contain PPCA, the PPCA-containing hydrogels can be distinguished from the surrounding tissue throughout the duration of the study. Without PPCA, hydrogels have similar signal intensities to surrounding tissue at the end of the gel lifetime. T_1 relaxation times support CNR data. This is the first report of use of a Gd(III)-based CA for detection of foreign body response to biomaterials, an essential property to assess before further material development. With incorporation of PPCAs, biomaterial improvement can be advanced through noninvasive in vivo assessment.

ACKNOWLEDGMENTS

The authors thank Dr. William Laskin for helpful discussions and Elise Sikma and Dr. Ying Song for ICP-MS

data acquisition. They thank Northwestern University's Institute for Bionanotechnology in Medicine, Pathology Core Facility, and Integrated Molecular Structure Education and Research Center for the use of instruments.

REFERENCES

1. Langer R, Tirrell DA. Designing materials for biology and medicine. Nature 2004;428:487–492.
2. Khor E, Hunt JA, Martin PA, Doherty PJ, Williams RL, Williams DF. Non-invasive magnetic resonance imaging of the soft tissue response to a biomaterial. Clin Mater 1993;12:65–72.
3. Cheng HLM, Wallis C, Shou Z, Farhat WA. Quantifying angiogenesis in VEGF-enhanced tissue-engineered bladder constructs by dynamic contrast-enhanced MRI using CAs of different molecular weights. J Magn Reson Imaging 2007;25:137–145.
4. Chen X, Astary GW, Sepulveda H, Mareci TH, Sarntinoranont M. Quantitative assessment of macromolecular concentration during direct infusion into an agarose hydrogel phantom using contrast-enhanced MRI. Magn Reson Imaging 2008;26:1433–1441.
5. Nitzsche H, Metz H, Lochmann A, Bernstein A, Hause G, Groth T, Mader K. Characterization of scaffolds for tissue engineering by benchtop-MRI. Tissue Eng Part C Methods 2009;15:513–521.
6. Choi HY, Lee JS, Park HJ, Oum BS, Kim HJ, Park DY. Magnetic resonance imaging assessment of fibrovascular ingrowth into porous polyethylene orbital implants. Clin Exp Ophthalmol 2006;34:354–359.
7. Miyata S, Numano T, Homma K, Tateishi T, Ushida T. Feasibility of noninvasive evaluation of biophysical properties of tissue-engineered cartilage by using quantitative MRI. J Biomech 2007;40:2990–2998.
8. Peptan IA, Hong L, Xu H, Magin RL. MR assessment of osteogenic differentiation in tissue-engineered constructs. Tissue Eng 2006;12:843–851.
9. Alikacem N, Marois Y, Zhang Z, Jakubiec B, Roy R, King MW, Guidoin R. Tissue reactions to polypyrrole-coated polyesters: a magnetic resonance relaxometry study. Artif Organs 1999;23:910–919.
10. Stroman PW, Dorvil JC, Marois Y, Poddevin N, Guidoin R. In vivo time course studies of the tissue responses to resorbable polylactic acid implants by means of MRI. Magn Reson Med 1999;42:210–214.
11. Traore AS, Woerly S, Doan VD, Marois Y, Guidoin R. In vivo magnetic resonance imaging and relaxometry study of a porous hydrogel implanted in the trapezius muscle of rabbits. Tissue Eng 2000;6:265–278.
12. Bull SR, Guler MO, Bras RE, Venkatasubramanian PN, Stupp SI, Meade TJ. Magnetic resonance imaging of self-assembled biomaterial scaffolds. Bioconjug Chem 2005;16:1343–1348.
13. Mader K, Bacic G, Domb AJ, Elmalak O, Langer R, Swartz HM. Non-invasive in vivo monitoring of drug release and polymer erosion from biodegradable polymers by EPR spectroscopy and NMR imaging. J Pharm Sci 1997;86:126–134.
14. Pihlajamaki H, Kinnunen J, Bostman O. In vivo monitoring of the degradation process of bioresorbable polymeric implants using magnetic resonance imaging. Biomaterials 1997;18:1311–1315.
15. Kim H, Lizak MJ, Tansey G, Csaky KG, Robinson MR, Yuan P, Wang NS, Lutz RJ. Study of ocular transport of drugs released from an intravitreal implant using magnetic resonance imaging. Ann Biomed Eng 2005;33:150–164.
16. Weissleder R, Poss K, Wilkinson R, Zhou C, Bogdanov AA. Quantitation of slow drug release from an implantable and degradable gentamicin conjugate by in vivo magnetic resonance imaging. Antimicrob Agents Chemother 1995;39:839–845.
17. Frullano L, Meade TJ. Multimodal MRI contrast agents. J Biol Inorg Chem 2007;12:939–949.
18. Wang X, Feng Y, Ke T, Schabel M, Lu Z. Pharmacokinetics and tissue retention of (Gd-DTPA)-cystamine copolymers, a biodegradable macromolecular magnetic resonance imaging contrast agent. Pharm Res 2004;22:596–602.
19. Jaszberenyi Z, Moriggi L, Schmidt P, Weidensteiner C, Kneuer R, Merbach AE, Helm L, Toth E. Physicochemical and MRI characterization of Gd3+-loaded polyamidoamine and hyperbranched dendrimers. J Biol Inorg Chem 2007;12:406–420.
20. Mohs AM, Lu ZR. Gadolinium(III)-based blood-pool contrast agents for magnetic resonance imaging: status and clinical potential. Exp Opin Drug Deliv 2007;4:149–164.
21. Song Y, Kohlmeir EK, Meade TJ. Synthesis of multimeric MR contrast agents for cellular imaging. J Am Chem Soc 2008;130:6662–6663.
22. Huber MM, Staubli AB, Kustedjo K, Gray MHB, Shih J, Fraser SE, Jacobs RE, Meade TJ. Fluorescently detectable magnetic resonance imaging agents. Bioconjug Chem 1998;9:242–249.
23. Karfeld-Sulzer LS, Waters EA, Davis NE, Meade TJ, Barron AE. Multivalent protein polymer MRI contrast agents: controlling relaxivity via modulation of amino acid sequence. Biomacromolecules 2010;11:1429–1436.
24. Davis NE, Ding S, Forster R, Pinkas DM, Barron AE. Modular enzymatically crosslinked protein polymer hydrogels for in situ gelation. Biomaterials 2010;31:7288–7297.
25. Davis NE, Karfeld-Sulzer LS, Ding S, Barron AE. Synthesis and characterization of a new class of cationic protein polymers for multivalent display and biomaterial applications. Biomacromolecules 2009;10:1125–1134.
26. Liu S, Tobias R, McClure S, Styba G, Shi Q, Jackowski G. Removal of endotoxin from recombinant protein preparations. Clin Biochem 1997;30:455–463.
27. Zhou X, Westland PO. The viscosity and temperature dependence of ^{1}H T_1-NMRD of the $Gd(H_2O)_8^{3+}$ complex. Spectrochim Acta A 2005;62:335–342.
28. Brandl F, Sommer F, Goepferich A. Rational design of hydrogels for tissue engineering: impact of physical factors on cell behavior. Biomaterials 2007;28:134–146.
29. Alsberg E, Kong HJ, Hirano Y, Smith MK, Albeiruti A, Mooney DJ. Regulating bone formation via controlled scaffold degradation. J Dent Res 2003;82:903–908.
30. Bryant SJ, Anseth KS. Controlling the spatial distribution of ECM components in degradable PEG hydrogels for tissue engineering cartilage. J Biomed Mater Res A 2003;64:70–79.
31. Kong HJ, Kaigler D, Kim K, Mooney DJ. Controlling rigidity and degradation of alginate hydrogels via a molecular weight distribution. Biomacromolecules 2004;5:1720–1727.
32. Meinel L, Hofmann S, Karageorgiou V, Zichner L, Langer R, Kaplan D, Vunjak-Novakovic G. Engineering cartilage-like tissue using human mesenchymal stem cells and silk protein scaffolds. Biotechnol Bioeng 2004;88:379–391.
33. Babensee JE, Anderson JM, McIntire LV, Mikos AG. Host response to tissue engineered devices. Adv Drug Deliv Rev 1998;33:111–139.
34. Crompton KE, Tomas D, Finkelstein DI, Marr M, Forsythe JS, Horne MK. Inflammatory response on injection of chitosan/GP to the brain. J Mater Sci Mater Med 2006;17:633–639.
35. Ling CR, Foster MA. Changes in NMR relaxation time associated with local inflammatory response. Phys Med Biol 1982;27:853–860.
36. Anderson JM. Biological responses to materials. Annu Rev Mater Res 2001;31:81–110.